CALCULATION OF TURBULENT SHEAR STRESS IN SUPERSONIC BOUNDARY LAYER FLOWS

by

Chen-Chih Sun*
and
Morris E. Childs+
University of Washington, Seattle, Washington

Turbulent shear stress distributions for supersonic boundary layer flows have been computed from experimental mean boundary layer data. The computations have been made by numerically integrating the time averaged continuity and streamwise momentum equations. The computational method is different from those previously reported in that integrated mass and momentum flux profiles and differentials of these integral quantities are used in the computations so that local evaluation of the streamwise velocity gradient is not necessary. Distributions have been obtained for flows upstream and downstream of shock wave-boundary layer interactions and for both two-dimensional and axisymmetric flows. The computed results are compared with recently reported shear stress measurements which were obtained by hot wire anemometer and laser velocimeter techniques. For most of the results shown reasonably good agreement is found

This work was supported by NASA Grant NGR-48-002-047 under administration of the Aerodynamics Branch, Ames Research Center.

Index Categories: Boundary layers and convective heat transfer
Turbulent supersonic and hypersonic flow
Shock waves

* Research Associate (Postdoctoral), Department of Mechanical Engineering, University of Washington, Seattle, Washington. Member AIAA.

+ Professor and Chairman, Department of Mechanical Engineering, University of Washington, Seattle, Washington. Member AIAA.

(NASA-CR-138659) CALCULATION OF TURBULENT SHEAR STRESS IN SUPERSONIC BOUNDARY LAYER FLOWS (Washington Univ.) 37 p HC $4.75 CSCL 20D G3/12 41362 Unclas N74-26799

between the computed and the measured results. The computed values of shear stress are quite sensitive to rather small differences in the mean flow properties of the boundary layer, indicating that exceptionally accurate mean flow data are required if reliable shear stress distributions are to be obtained from the mean data. Computations have also been made of eddy viscosity and mixing length distributions. These are compared with results based on the direct measurements of shear stress.

SYMBOLS

a = a constant, see Eq. (13)

C = constant in Law of the Wall (usually equals 5.1)

C_f = skin friction coefficient

K = a constant, see Eq. (13)

k = a constant, see Eq. (18)

ℓ = mixing length, see Eq. (17)

M = Mach number

P = pressure

r = distance normal to centerline

R = radius of the duct

T_{ij} = total stress tensor

u = time averaged velocity in primary flow direction

u^* = $(u_e/\sigma^{1/2})$ arc sin $(\sigma^{1/2}\ u/u_e)$

u_τ = friction velocity $(\tau_w/\rho_w)^{1/2}$

v = time averaged velocity normal to centerline

x = distance parallel to centerline.

y = R-r

γ = ratio of specific heat (1.4 for present study)

δ = boundary layer thickness

ε = eddy viscosity

μ = molecular viscosity

η = y/δ

Π = coefficient of wake function, see Eq. (13)

ρ = time averaged density

σ = $[(\gamma-1)/2]M_e^2 / \{1 + [(\gamma-1)/2]\ M_e^2\}$

τ = shear stress

Subscripts

e = boundary layer edge condition

w = wall condition

∞ = free stream condition

Superscript

<( )'>= time averaged fluctuation value

I. INTRODUCTION

In the study of supersonic turbulent boundary layer flow the turbulent shear stress distribution has always been of great importance and interest. The direct measurement of the turbulent shear stress is, however, quite difficult. A natural alternative is to compute the shear from experimental mean flow data by numerically integrating the momentum equation. Such computations have been performed in recent studies by Bushnell and Morris[1], Horstman and Owen[2], and Sturek[3]. Since directly measured data with which to compare the computed results were not available, it was not possible to check the validity of the computations nor of simplifying assumptions made in connection with the computations.

Recently, some turbulent shear stress data measured directly by using hot wire anemometer and laser velocimeter techniques have been reported by Rose and Johnson[4,5]. The measurements were made upstream and downstream of an adiabatic unseparated interaction of an oblique shock wave with the turbulent boundary layer on the flat wall of a two-dimensional, $M_\infty = 2.9$ wind tunnel. The shock wave was generated by a 7° wedge. The turbulence data obtained from the two independent systems of measurement were in reasonably good agreement, indicating that the data should be reliable.

In another study by Rose[6] of the interaction of a conical shock wave with a turbulent boundary layer on the wall section of an axisymmetric wind tunnel, a hot wire anemometer has been used to make measurements of the turbulent shear stress and other turbulence quantities. The flow was adiabatic. For both of these investigations the turbulent

shear stress distributions at stations upstream and downstream of the shock wave-boundary layer interaction have been computed from the mean flow pitot pressure profiles obtained in the studies. Eddy viscosity and mixing length distributions have also been computed for the two flows. For the two-dimensional interaction investigated by Rose and Johnson[4,5], computed results show reasonably good agreement with the results obtained by direct measurement. For the axisymmetric flow studied by Rose[6] computed and measured results show good agreement upstream of the interaction but differ considerably at the downstream station.

II. BASIC EQUATIONS AND BOUNDARY CONDITIONS

The time-averaged equations for the conservation of mass and momentum for steady compressible turbulent boundary layer flow in an axisymmetric channel are, respectively,

$$\frac{\partial}{\partial x}(\rho u) + \frac{\partial}{\partial x}\langle \rho' u' \rangle + \frac{1}{r}\frac{\partial}{\partial r}(r\rho v) + \frac{1}{r}\frac{\partial}{\partial r}(r\langle \rho' v' \rangle) = 0 \tag{1}$$

and

$$\frac{\partial}{\partial x}(\rho u^2) + \frac{1}{r}\frac{\partial}{\partial r}(r\rho uv) = -\frac{\partial P}{\partial x} + \frac{\partial}{\partial x}T_{xx} + \frac{1}{r}\frac{\partial}{\partial r}T_{rx} \tag{2}$$

where

$$T_{xx} = (\tau_v)_{xx} - (\rho\langle u'^2 \rangle + 2u\langle \rho' u' \rangle) \tag{3}$$

$$T_{rx} = (\tau_v)_{rx} - (\rho\langle u'v' \rangle + u\langle \rho' v' \rangle + v\langle \rho' u' \rangle) \tag{4}$$

with τ_v representing the viscous stress.

If we assume that $|v \langle \rho' u' \rangle| \ll |\rho \langle u' v' \rangle|$ and $|\frac{\partial}{\partial x} \langle \rho' u' \rangle| \ll |\frac{\partial}{\partial x} (\rho u)|$ and transform to an x-y coordinate system the continuity and momentum equations may be combined and integrated in a direction normal to the surface to yield

$$\frac{\tau}{\rho_e u_e^2} \left(1 - \frac{y}{R}\right) = \frac{C_f}{2} + \frac{1}{\rho_e u_e^2 R} \int_o^y \frac{\partial}{\partial x} [\rho u^2 (R-y)] \, dy$$

$$- \frac{u}{\rho_e u_e^2 R} \int_o^y \frac{\partial}{\partial x} [\rho u (R-y)] \, dy + \frac{1}{\rho_e u_e^2 R} \int_o^y (R-y) \frac{\partial}{\partial x} (p - T_{xx}) \, dy \qquad (5)$$

where

$$y = R - r \qquad (6)$$

and

$$\tau = \mu \frac{\partial u}{\partial y} - \rho \langle u' v' \rangle \qquad (7)$$

Rearrangement of equation (5) gives

$$\frac{\tau}{\rho_e u_e^2} \left(1 - \eta \frac{\delta}{R}\right) = \frac{C_f}{2} + \left(\frac{d\delta}{dx} + \frac{\delta}{\rho_e u_e^2} \frac{d\rho_e u_e^2}{dx} + \frac{\delta}{R} \frac{dR}{dx}\right) \int_o^\eta \frac{\rho u^2}{\rho_e u_e^2} \, d\eta$$

$$- \left(\frac{2\delta}{R} \frac{d\delta}{dx} + \frac{\delta^2}{\rho_e u_e^2 R} \frac{d\rho_e u_e^2}{dx}\right) \int_o^\eta \eta \frac{\rho u^2}{\rho_e u_e^2} \, d\eta$$

$$- \left(\frac{d\delta}{dx} + \frac{\delta}{R} \frac{dR}{dx} + \frac{\delta}{\rho_e u_e} \frac{d\rho_e u_e}{dx}\right) \frac{u}{u_e} \int_o^\eta \frac{\rho u}{\rho_e u_e} \, d\eta$$

$$+ \left(\frac{2\delta}{R}\frac{d\delta}{dx} + \frac{\delta^2}{\rho_e u_e R}\frac{d\rho_e u_e}{dx}\right)\frac{u}{u_e}\int_o^\eta \eta\,\frac{\rho u}{\rho_e u_e}\,d\eta$$

$$+ \delta\,\frac{\partial}{\partial x}\int_o^\eta \frac{\rho u^2}{\rho_e u_e^2}\,d\eta - \frac{\delta^2}{R}\frac{\partial}{\partial x}\int_o^\eta \eta\,\frac{\rho u^2}{\rho_e u_e^2}\,d\eta$$

$$- \delta\,\frac{u}{u_e}\frac{\partial}{\partial x}\int_o^\eta \frac{\rho u}{\rho_e u_e}\,d\eta + \frac{u}{u_e}\frac{\delta^2}{R}\frac{\partial}{\partial x}\int_o^\eta \eta\,\frac{\rho u}{\rho_e u_e}\,d\eta$$

$$+ \frac{\delta}{\rho_e u_e^2 R}\int_o^\eta (R-\eta\delta)\left(\frac{\partial p}{\partial x} - \frac{\partial}{\partial x}T_{xx}\right)d\eta \qquad (8)$$

Equation (8) becomes applicable to two-dimensional flow as $R \to \infty$.

The normal stress, T_{xx}, which appears in equation (8), is not known from mean profile data. If its effect is to be considered in the computations, it is necessary then to make assumptions regarding its magnitude. In earlier studies, and for most of the results to be discussed here, the streamwise gradient of T_{xx} has been neglected. However, by assigning arbitrary values to the T_{xx} derivative, its effect on the computed results may be examined. This has been done in one instance as will be discussed in the section on results.

Knowledge is also required of the static pressure distribution in the boundary layer. In many studies of supersonic boundary layer flow no attempt is made to measure the static pressure variation normal to the wall, even though, for some adverse pressure gradient flows, the variation may, in fact, be rather large. In most instances the static pressure at the boundary layer edge may be determined with confidence. If this is done, the normal pressure variation may then be represented in approximate fashion by assuming a linear distribution between the wall static pressure and the pressure at the boundary layer edge, i.e.,

$$p = p_w + \eta(p_e - p_w) \tag{9}$$

Examination of equation (8) shows that an accurate value of boundary layer growth rate is very important for the calculation of the shear stress. However, precise determination of the boundary layer thickness from experimental mean data is difficult. It is even more difficult to evaluate the boundary layer growth rate accurately. This problem may be avoided by using the condition that the shear stress diminishes to zero at the boundary layer edge and solving equation (8) for $d\delta/dx$:

$$\begin{aligned}
\frac{d\delta}{dx} = \Bigg[& \frac{C_f}{2} + \left(\frac{\delta}{\rho_e u_e^2}\frac{d\rho_e u_e^2}{dx} + \frac{\delta}{R}\frac{dR}{dx}\right)\int_o^1 \frac{\rho u^2}{\rho_e u_e^2}\,d\eta \\
& - \frac{\delta^2}{\rho_e u_e^2 R}\frac{d\rho_e u_e^2}{dx}\int_o^1 \eta\,\frac{\rho u^2}{\rho_e u_e^2}\,d\eta \\
& - \left(\frac{\delta}{R}\frac{dR}{dx} + \frac{\delta}{\rho_e u_e}\frac{d\rho_e u_e}{dx}\right)\int_o^1 \frac{\rho u}{\rho_e u_e}\,d\eta + \frac{\delta^2}{\rho_e u_e R}\frac{d\rho_e u_e}{dx}\int_o^1 \eta\,\frac{\rho u}{\rho_e u_e}\,d\eta \\
& + \delta\frac{\partial}{\partial x}\int_o^1 \frac{\rho u^2}{\rho_e u_e^2}\,d\eta - \frac{\delta^2}{R}\frac{\partial}{\partial x}\int_o^1 \eta\,\frac{\rho u^2}{\rho_e u_e^2}\,d\eta - \delta\frac{\partial}{\partial x}\int_o^1 \frac{\rho u}{\rho_e u_e}\,d\eta \\
& + \frac{\delta^2}{R}\frac{\partial}{\partial x}\int_o^1 \eta\,\frac{\rho u}{\rho_e u_e}\,d\eta + \frac{\delta}{\rho_e u_e^2}\frac{dP_w}{dx}\left(1 - \frac{\delta}{2R}\right) \\
& + \frac{\delta}{\rho_e u_e^2}\frac{d(P_e - P_w)}{dx}\left(\frac{1}{2} - \frac{\delta}{3R}\right)\Bigg] \Big/ \Bigg[\frac{2\delta}{R}\int_o^1 \eta\,\frac{\rho u}{\rho_e u_e^2}\,d\eta \\
& - \int_o^1 \frac{\rho u^2}{\rho_e u_e^2}\,d\eta + \int_o^1 \frac{\rho u}{\rho_e u_e}\,d\eta - \frac{2\delta}{R}\int_o^1 \eta\,\frac{\rho u}{\rho_e u_e}\,d\eta \\
& + \frac{(P_e - P_w)}{\rho_e u_e^2}\left(\frac{1}{2} - \frac{\delta}{3R}\right)\Bigg]
\end{aligned} \tag{10}$$

In equation (10) a linear pressure variation normal to the wall has been assumed.

If the streamwise gradient of the normal stress is ignored and if the flow is assumed to be locally similar so that the nondimensional boundary layer properties u/u_e and ρ/ρ_e are functions of η only, equation (8) reduces to

$$\frac{\tau}{\rho_e u_e^2}\left(1 - \eta\frac{\delta}{R}\right) = \frac{C_f}{2} + \left(\frac{d\delta}{dx} + \frac{\delta}{\rho_e u_e^2}\frac{d\rho_e u_e^2}{dx} + \frac{\delta}{R}\frac{dR}{dx}\right)\int_o^\eta \frac{\rho u^2}{\rho_e u_e^2}\,d\eta$$

$$- \left(\frac{2\delta}{R}\frac{d\delta}{dx} + \frac{\delta^2}{\rho_e u_e^2 R}\frac{d\rho_e u_e^2}{dx}\right)\int_o^\eta \eta\,\frac{\rho u^2}{\rho_e u_e^2}\,d\eta$$

$$- \left(\frac{d\delta}{dx} + \frac{\delta}{R}\frac{dR}{dx} + \frac{\delta}{\rho_e u_e}\frac{d\rho_e u_e}{dx}\right)\frac{u}{u_e}\int_o^\eta \frac{\rho u}{\rho_e u_e}\,d\eta$$

$$+ \left(\frac{2\delta}{R}\frac{d\delta}{dx} + \frac{\delta^2}{\rho_e u_e R}\frac{d\rho_e u_e}{dx}\right)\frac{u}{u_e}\int_o^\eta \eta\,\frac{\rho u}{\rho_e u_e}\,d\eta$$

$$+ \frac{\delta}{\rho_e u_e^2 R}\int_o^\eta (R - \eta\delta)\,\frac{\partial P}{\partial x}\,d\eta \qquad (11)$$

and equation (10) becomes

$$\frac{\partial\delta}{\partial x} = \left[\frac{C_f}{2} + \left(\frac{\delta}{\rho_e u_e^2}\frac{d\rho_e u_e^2}{dx} + \frac{\delta}{R}\frac{dR}{dx}\right)\int_o^1 \frac{\rho u^2}{\rho_e u_e^2}\,d\eta\right.$$

$$- \frac{\delta^2}{\rho_e u_e^2 R}\frac{d\rho_e u_e^2}{dx}\int_o^1 \eta\,\frac{\rho u^2}{\rho_e u_e^2}\,d\eta - \left(\frac{\delta}{R}\frac{dR}{dx} + \frac{\delta}{\rho_e u_e}\frac{d\rho_e u_e}{dx}\right)\int_o^1 \frac{\rho u}{\rho_e u_e}\,d\eta$$

$$\left. + \frac{\delta^2}{\rho_e u_e R}\frac{d\rho_e u_e}{dx}\int_o^1 \frac{\rho u}{\rho_e u_e}\,d\eta + \frac{\delta}{\rho_e u_e^2}\frac{dP_w}{dx}\left(1 - \frac{\delta}{2R}\right)\right.$$

$$+ \frac{\delta}{\rho_e u_e^2} \frac{d(P_e - P_w)}{dx} \left(\frac{1}{2} - \frac{\delta}{3R}\right)\Big] \Big/ \left[\frac{2\delta}{R} \int_o^1 \eta \, \frac{\rho u^2}{\rho_e u_e^2} \, d\eta \right.$$

$$\left. - \int_o^1 \frac{\rho u^2}{\rho_e u_e^2} \, d\eta + \int_o^1 \frac{\rho u}{\rho_e u_e} \, d\eta - \frac{2\delta}{R} \int_o^1 \eta \, \frac{\rho u}{\rho_e u_e} \, d\eta \right] \tag{12}$$

Equation (11) is identical to the expression used by Bushnell and Morris[1] in their computations of turbulent shear stress.

Before solving for the shear stress from either equation (8) or (11) it is also necessary to know the coefficient of skin friction. This may be obtained by using the wall-wake velocity profile proposed by Sun and Childs[7]. The wall-wake velocity profile for isoenergetic flow may be written as

$$\frac{u}{u_e} = \frac{1}{\sigma^{1/2}} \sin \left\{ \arcsin \sigma^{1/2} \left[1 + \frac{1}{K} \frac{u_\tau}{u_e^*} \left(\ln \eta + \frac{2(1-\eta^a)^{1/2}}{a} \right. \right. \right.$$

$$\left. \left. \left. - \frac{2}{a} \ln \left(1 + (1-\eta^a)^{1/2}\right) - \frac{\Pi}{K} \frac{u_\tau}{u_e^*} \left(1 + \cos \eta \pi\right) \right] \right\} \tag{13}$$

where

$$\frac{\Pi}{K} = \frac{1}{2} \left[\frac{u_e^*}{u_\tau} - \frac{1}{K} \ln \left(\frac{\delta u_\tau}{\nu_w} \right) - 5.1 + \frac{0.614}{aK} \right] \tag{14}$$

and

$$\frac{u_\tau}{u_e^*} = \left(\frac{C_f}{2} \frac{\sigma}{1-\sigma} \right)^{1/2} \arcsin \sigma^{1/2} \tag{15}$$

As has been reported in Reference 7, the use of $a = 1$ in equations (13) and (14) results in a profile which provides a good representation of the boundary layer velocity distribution. The method of least-squares may be

used to fit the wall-wake profile to the experimental mean velocity profiles to provides values of C_f and to provide a smoothed representation of the mean velocity distribution.

The eddy viscosity and mixing length distributions are also of great interest in the study of turbulent boundary layer flow. In terms of the shear stress as computed from mean flow data, the eddy viscosity may be written as

$$\frac{\varepsilon}{u_e \delta} = \frac{1}{u_e \delta} \left(\frac{\tau - \mu \, \partial u/\partial y}{\rho \, \partial u/\partial y} \right) \tag{16}$$

and the mixing length as

$$\frac{\ell}{\delta} = \frac{1}{\delta} \left[\frac{\tau - \mu \, \partial u/\partial y}{\rho (\partial u/\partial y)^2} \right]^{1/2} \tag{17}$$

In the region close to the wall the mixing length may be approximated by

$$\ell = ky \tag{18}$$

where k is a constant.

In terms of turbulence measurements the eddy viscosity may be expressed as

$$\frac{\varepsilon}{u_e \delta} = \left(\frac{1}{u_e \delta} \right) \left(\frac{-\langle u'v' \rangle}{\partial u/\partial y} \right) \tag{19}$$

and the mixing length as

$$\frac{\ell}{\delta} = \frac{1}{\delta} \left[\frac{-\langle u'v' \rangle}{(\partial u/\partial y)^2} \right]^{1/2} . \tag{20}$$

A comparison of eddy viscosity and mixing length values as determined from turbulence measurements and from mean flow shear stress computations is given in the section on results.

III. RESULTS

A computer program has been developed to carry out the required numerical calculations. In carrying out the computations for the flow downstream of the shock wave-boundary layer interactions, the departure from local similarity has been taken into account. For purposes of comparison, however, computations based on local similarity have also been made. The effect of static pressure variation normal to the wall has also been considered for the downstream stations by assuming a linear variation in pressure. In these computations the static pressure at the boundary layer edge has been computed from the free stream total pressure and pitot pressure, with appropriate allowance made for the loss in total pressure across the shock system. As was mentioned in the previous section, the mean velocity profiles may be smoothed by using a least squares fit of the wall-wake velocity profile to the experimental profiles. Computations have been made for both smoothed and unsmoothed profiles. The integration process for the smoothed data should be more accurate because it is possible to use smaller step sizes. On the other hand, the shear stress computed from the smoothed profiles is valid only if the wall-wake profile provides a good representation of the actual velocity distribution.

In obtaining the density and velocity profiles from the pitot pressure profiles for the investigation by Rose and Johnson[4,5], the total temperature was assumed to be constant across the boundary layer. In the axisymmetric study by Rose[6] total temperature measurements were available. For this case calculations of the shear stress distributions were made for both the measured total temperature distribution and for a constant total temperature. The results differed from each other only slightly.

Figure 1 shows shear stress distributions computed for an upstream ($x = 5.375$ cm) station in Johnson's and Rose's investigation, along with their shear stress data from the hot-wire anemometer and the laser velocimeter measurements. The computed shear values which are shown have been obtained from equation (11) and auxiliary equation (12), i.e., under the assumption of local similarity. As is shown the calculated results agree quite well over much of the boundary layer, with the measured results obtained with the laser velocimeter. The differences between the calculated results and the hot-wire results are greater. For both the hot-wire and laser velocimeter measurements the peak values of shear stress are seen to occur substantially farther from the wall than is observed for the calculated distributions. Also shown in the figure are values of the wall shear stress as determined by a least squares fit of the wall-wake profile to the mean data and as measured by a Preston tube. The agreement between the two shear stress values is good.

The wall-wake profile as given by equation (13) can be reduced to a profile proposed earlier by Maise and McDonald[8] if Π is taken to be equal to 5.0 and if $a \to \infty$. For purposes of comparison, the Maise-McDonald profile has been used to compute shear stress values. As is shown, this results in shear values which are substantially lower than those obtained with $a = 1$ in equation (13) or with the unsmoothed data.

Computations have also been carried out for the data of Rose and Johnson for a station downstream of the shock wave-boundary layer interaction ($x = 9.375$ cm). Several sets of computations have been made from the mean data. In one set local similarity has been assumed. Equations (11) and (12) have then been used to carry out computations for both

wall-wake smoothed profile and a profile as measured. In other computations local similarity of profiles has not been assumed. For these cases results have been obtained for both smoothed and unsmoothed profiles and both linear and constant static pressure distribution across the boundary layer. The results are shown in Figures 2 and 3. Figure 2 shows that the measured shear stress values obtained by the two experimental techniques are in quite good agreement. These in turn agree reasonably well with the computed values obtained by using smoothed nonsimilar profiles and the assumption of a linear pressure variation across the boundary layer. There is considerable difference between the results for the smoothed and unsmoothed profiles with the peak shear stress value for the unsmoothed profile occurring lower in the boundary layer. As was stated earlier, the numerical integration process should be more accurate for the smoothed profiles. On the other hand, the results obtained from the wall-wake profiles are valid only if the profiles provide accurate representations of the actual velocity distributions. A comparison of the computed velocity distributions with the corresponding wall-wake profiles is shown in Figure 4. The differences between the two are small, pointing to the sensitivity of the computed shear stress values to small velocity differences.

As is shown in Figure 3, the results obtained under the assumption of local similarity are markedly different from those determined when similarity is not assumed. The peak shear stress levels computed assuming local similarity are less than half the values computed when similarity is not assumed. Furthermore, the shapes of the shear stress distribution curves are quite different. These results occur even though the differences

between profiles at two closely spaced stations are small. Figure 5 shows comparisons of density and velocity profiles from Rose's and Johnson's study for streamwise stations located approximately one boundary layer thickness apart. Although the profiles appear at first glance to be quite similar, striking differences are found for the computed shear stress distributions.

In the investigation by Rose[6] of an adiabatic axisymmetric shock wave-boundary layer interaction the free stream flow was nominally at M = 4 and the shock wave was generated by a 9-degree half-angle cone placed at zero angle of attack on the centerline of the 5.28 cm diameter tunnel. The shock strength was just below that required to produce boundary layer separation. For this flow a substantial adverse pressure gradient existed downstream of the interaction. As was stated earlier, the turbulence data were obtained with a hot-wire anemometer.

Figure 6 shows results for a station upstream of the interaction where there was no pressure gradient. The shear stress distribution has been computed from mean velocity and density profiles under the assumption of local similarity and constant static pressure across the boundary layer. As is shown, reasonably good agreement between computed and measured shear stress values is obtained, although the differences observed for the Rose-Johnson[4,5] data are found to exist here as well. That is, the hot-wire anemometer results show higher levels than the computed values in the outer part of the boundary layer, and the peak value of the computed shear stress is much closer to the wall than was found to be the case from the direct measurements.

Figure 7 shows results for a station (at x = 10.16 cm) downstream of the interaction. As was the case with the Rose-Johnson investigation, several sets of computations have been made from the mean data. For all the results shown the assumption of a linear static pressure variation across the boundary layer has been assumed. Results have been obtained for both smoothed and unsmoothed profiles, and computations have been carried out for both local similarity and nonsimilarity of velocity and density profiles. In addition, allowance has been made in one set of calculations for the streamwise gradient of the normal stress, $\partial T_{xx}/\partial x$. Johnson and Rose found in their study of the two-dimensional interaction that this gradient was small and no allowance was made for it in the computations. However, for the axisymmetric flow Rose reported that streamwise normal stress gradient reached levels as high as 30 percent of the local streamwise pressure gradient. The distribution of normal stress gradient as reported by Rose may be represented approximately by

$$\frac{\partial T_{xx}}{\partial x} = 0.3 \frac{\partial P}{\partial x} \sin^2 \eta\pi \tag{21}$$

Computations have been made assuming the distribution given by equation (21).

As is shown in Figure 7, the difference between the measured and computed shear stress values is substantial. The peak value of the measured shear stress is about twice the peak value computed when local similarity is not assumed. As was true for the downstream station in the Rose-Johnson study, peak levels of the computed shear stress are seen to occur

considerably closer to the wall than is observed in the measurements. It has not yet been possible to determine the causes for the rather large differences between the peak levels of the computed and measured shear stress distributions. Additional hot-wire studies are underway for the axisymmetric flow, as are attempts to improve upon the computational techniques.

As was the case for the downstream station in the Rose-Johnson[4,5] investigation, the assumption of local similarity leads to shear stress levels which are on the order of only one-half those determined when similarity is not assumed. As is shown in Figure 7, consideration of the streamwise normal stress gradient in the computations results in shear stress levels which differ only very slightly from those obtained when the gradient is ignored.

It should be pointed out that Rose[6], in obtaining his downstream data, moved the cone along the axis of the tunnel and obtained the pitot measurements at a fixed axial station. The question arises, then, of how the computed shear stress distributions would compare with those obtained if the cone had been kept at one station and the pitot tube had been traversed axially. As a check on this, data were examined from a study by Seebaugh[9] in which the cone was held fixed and the probe was translated. Seebaugh's study was conducted in a 5.16 cm diameter round tunnel with a free-stream Mach number of 3.78. He used a 10-degree half-angle cone. The results are shown in Figure 8. As is apparent, the shear stress distributions are quite comparable to those obtained from Rose's mean flow data.

The distributions of eddy viscosity and mixing length for the investigations under consideration are shown in Figures 9-12. The results, of course, reflect the differences between the measured and computed values of shear stress as discussed earlier. Computed results are shown for both smoothed and unsmoothed profiles. For the stations upstream of the shock wave-boundary layer interactions the shear stress distributions used in obtaining the values of eddy viscosity and mixing length have been determined under the assumption of local similarity. For the downstream stations, the lack of local similarity in the velocity and density profiles has been taken into account and a linear static pressure variation across the boundary layer has been assumed.

The eddy viscosity distributions for the Rose-Johnson investigation are shown in Figure 9. Near the wall moderately good agreement is observed between eddy viscosities based on computed shear stress values and those based on measurements. From $y/\delta = 0.2$ outward, however, the differences become substantial. The values based on experimental shear stress show considerable scatter as do those based on the point-by-point mean data. In contrast the results based on the wall-wake smoothed velocity profile are smooth, as would be expected.

The mixing length distributions for the Rose-Johnson[4,5] investigation are shown in Figure 10. Near the wall the values of mixing length are described reasonably well by the relationship $\ell = 0.4y$. From $y/\delta = 0.2$ outward a certain amount of scatter in the results is apparent. For the upstream station ($x = 5.375$ cm), however, the computed distribution based on the wall-wake profile agrees with the results based on turbulence measurements reasonably well. For the downstream station ($x = 9.375$ cm) the

values of ℓ/δ based on the wall-wake profile are consistently higher than those based on the turbulence measurements or on the unsmoothed mean data.

The eddy viscosity distributions for the axisymmetric flows studied by Rose[6] and by Seebaugh[9] are shown in Figure 11. As is shown the results based on the shear stresses computed from the mean flow data of Rose and Seebaugh are in good agreement. The values based on Rose's hot-wire anemometer measurements are much higher, consistent with the higher shear stresses which he reported.

Mixing length distributions for the downstream stations in Rose's and Seebaugh's investigations are shown in Figure 12, along with the results based on Rose's hot-wire anemometer measurements. Again the results agree well with the expression $\ell = 0.4y$ for the region near the wall. This is in contrast to the result reported by Sturek[3] who concluded for adverse pressure gradient flow $\ell = 0.65y$ appeared to fit his data near the wall. Sturek's studies were conducted for flow along a compression surface. The computed values of mixing length, ℓ/δ, in the plateau region are considerably different for the two-dimensional flow and the axisymmetric flows. Upstream of the shock wave interaction, the value is about 0.07 for axisymmetric flow while the value is about 0.12 for the two-dimensional flow. The computed values downstream of the interaction are somewhat higher than those upstream for both the two-dimensional and axisymmetric flows.

IV. CONCLUSIONS

A method of computing shear stress distribution from experimental mean profile data in compressible turbulent boundary layer flow has been developed. The method is different from those previously reported in that integrated mass and momentum flux profiles and differentials of these integral quantities are used in the computations so that local evaluation of the streamwise velocity gradient is not necessary. The method has been found to yield results which are in reasonably good agreement with directly measured turbulence data for two-dimensional adiabatic boundary layer flow in the regions upstream and downstream of an oblique shock wave interaction. The computed results are very sensitive to the accuracy of the numerical integrations required in the computational procedure and to the mean property distributions in the boundary layer. The assumption of local similarity may cause large errors in computed shear stress values for flows subjected to pressure gradients, even though adjacent profiles of the mean properties appear to be quite similar. The shear stress levels are quite sensitive to the static pressure distribution normal to the wall. The effect of the streamwise gradient of the normal stress on the computed results is small and apparently may be neglected. The value of the constant k in the expression $\ell = ky$ for the mixing length in the region near the wall remains close to 0.4 for adverse pressure gradient flows along a flat surface. In view of the rather substantial differences between results based on mean flow measurements and those based on turbulence measurements in an axisymmetric adverse pressure gradient flow, further study of this flow is needed.

REFERENCES

1. Bushnell, D.M. and Morris, D.J., "Shear-Stress, Eddy-Viscosity and Mixing Length Distributions in Hypersonic Turbulent Boundary Layers," NASA TMX-2310, 1971.

2. Horstman, C.C. and Owen, F.K., "Turbulent Properties of a Compressible Boundary Layer," AIAA Journal, vol. 10, no. 11, November 1972, pp. 1418-1424.

3. Sturek, W.B., "Calculations of Turbulent Shear Stress in Supersonic Turbulent Boundary Layer Zero and Adverse Pressure Gradient Flow," AIAA Paper No. 73-166, January 1973.

4. Johnson, D.A. and Rose, W.C., "Measurement of Turbulent Transport Properties in a Supersonic Boundary-Layer Flow Using Laser Velocimeter and Hot Wire Anemometer Techniques," AIAA Paper 73-1045, Seattle, Washington, 1973.

5. Rose, W.C. and Johnson, D.A., "A Study of Shock Wave Turbulent Boundary Layer Interaction Using Laser Velocimeter and Hot Wire Anemometer Techniques," AIAA Paper 74-95, Washington, D.C., 1974.

6. Rose, W.C., "The Behavior of a Compressible Turbulent Boundary Layer in a Shock-Wave-Induced Adverse Pressure Gradient," TND-7092, NASA, March 1973.

7. Sun, C.C. and Childs, M.E., "A Modified Wall-Wake Velocity Profile for Turbulent Compressible Boundary Layers," Journal of Aircraft, vol. 10, no. 6, June 1973, pp. 381-383.

8. Maise, G. and McDonald, H., "Mixing Length and Kinematic Eddy Viscosity in a Compressible Boundary Layer," AIAA Journal, vol. 6, no. 1, January 1968, pp. 73-80.

9. Seebaugh, W.R., "An Investigation of the Interaction of a Shock Wave and a Turbulent Boundary Layer in Axially Symmetric Internal Flow Including the Effect of Mass Bleed," PhD Thesis, 1968, University of Washington, Seattle, Washington.

Figure 1. Turbulent shear stress distribution upstream of a shock wave-boundary layer interaction, two-dimensional tunnel [4]

Figure 2. Turbulent shear stress distribution downstream of a shock wave-boundary layer interaction, two-dimensional tunnel [5]

Figure 3. Effect of static pressure distribution and self-similarity on shear stress distribution in a turbulent boundary layer downstream of a shock wave interaction [5]

Figure 4. Velocity profiles and wall-wake representations downstream of a shock wave-boundary layer interaction [5]

Figure 5. Density and velocity profiles downstream of a shock wave-boundary layer interaction [5]

Figure 6. Turbulent shear stress distribution upstream of a shock wave-boundary layer interaction, axisymmetric tunnel [6]

Figure 7. Turbulent shear stress distribution downstream of a shock wave-boundary layer interaction, axisymmetric tunnel [6]

Figure 8. Turbulent shear stress distribution downstream of a shock wave-boundary layer interaction, axisymmetric tunnel [9]

Figure 9. Eddy viscosity distribution for the two-dimensional flow of Rose and Johnson [4,5]

Figure 10. Mixing length distribution for the two-dimensional flow of Rose and Johnson [4,5]

Figure 11. Eddy viscosity distributions for the axisymmetric flows of Rose [6] and Seebaugh [9]

Figure 12. Mixing length distributions for the axisymmetric flows of Rose [6] and Seebaugh [9]

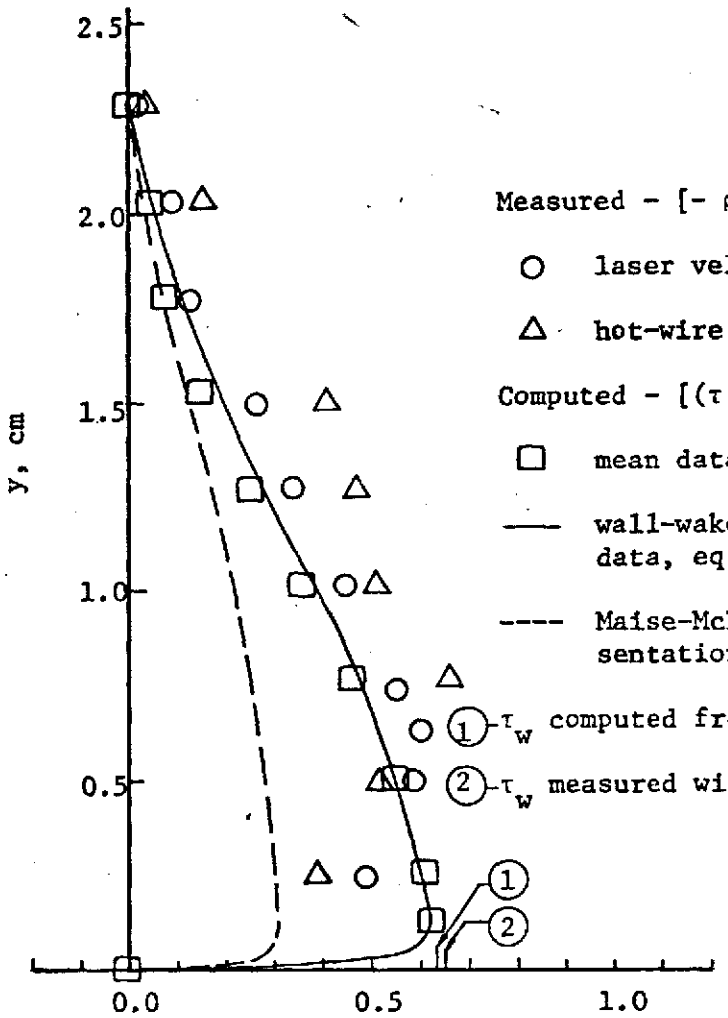

$[- \rho\langle u'v'\rangle/\rho_e u_e^2] \times 10^3$, $[(\tau - \mu\, \partial u/\partial y)/\rho_e u_e^2] \times 10^3$

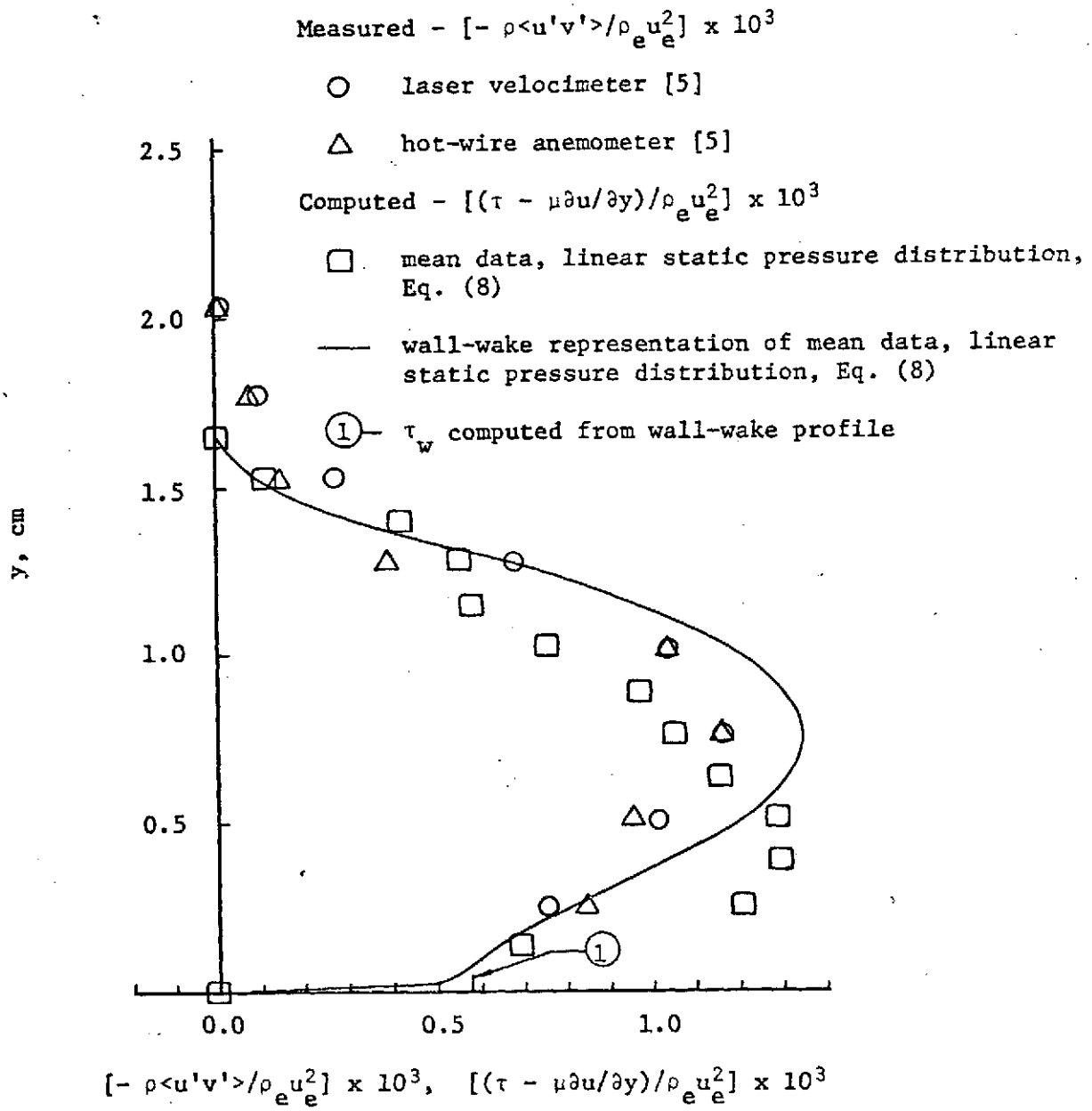
Measured - $[-\rho\langle u'v'\rangle/\rho_e u_e^2] \times 10^3$
laser velocimeter [5]
hot-wire anemometer [5]
Computed - $[(\tau - \mu\partial u/\partial y)/\rho_e u_e^2] \times 10^3$
mean data, linear static pressure distribution, Eq. (8)
wall-wake representation of mean data, linear static pressure distribution, Eq. (8)
1 τ_w computed from wall-wake profile
y, cm
2.5
2.0
1.5
1.0
0.5
0.0
0.5
1.0
$[-\rho\langle u'v'\rangle/\rho_e u_e^2] \times 10^3$, $[(\tau - \mu\partial u/\partial y)/\rho_e u_e^2] \times 10^3$

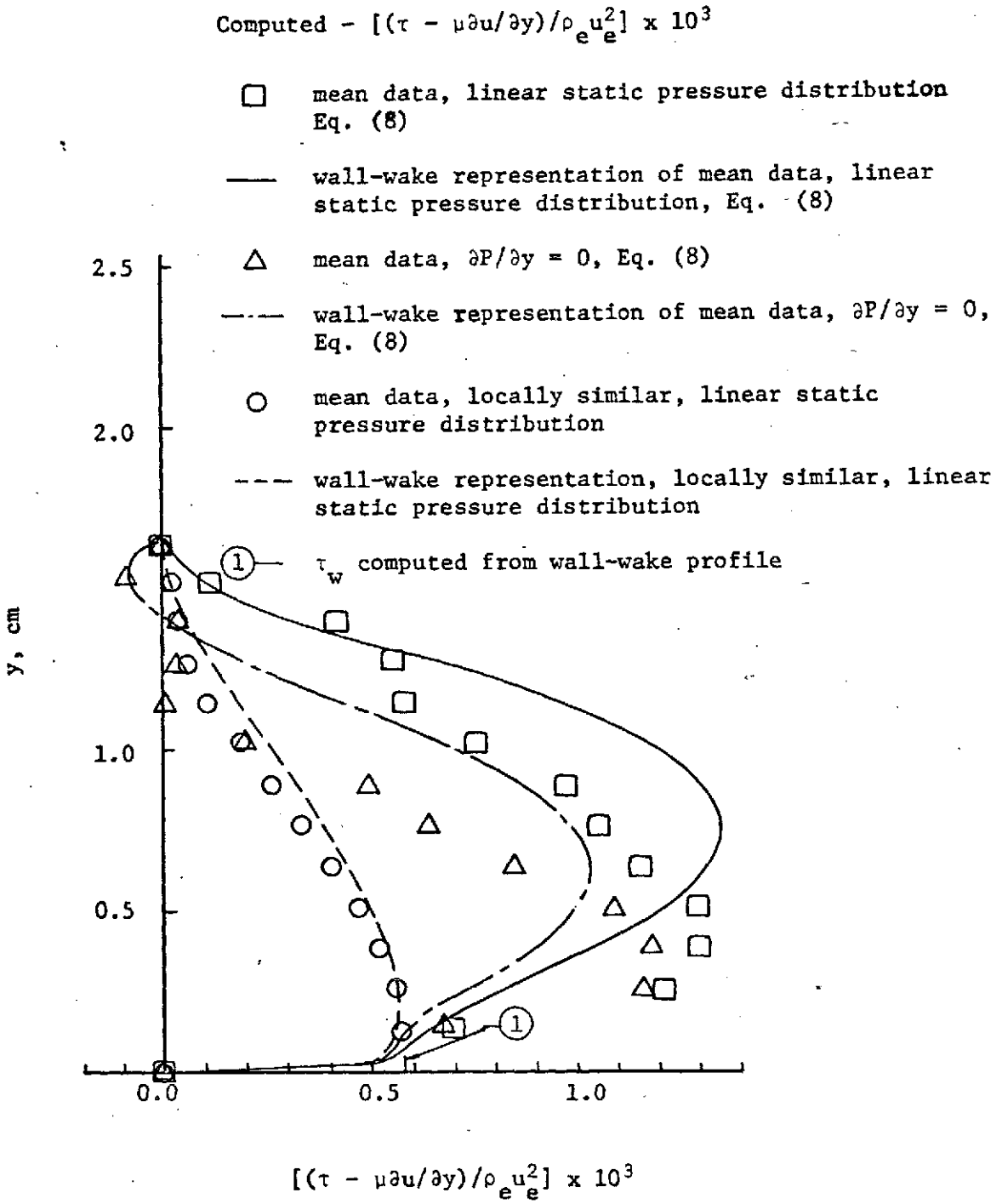
Computed - $[(\tau - \mu\partial u/\partial y)/\rho_e u_e^2] \times 10^3$
mean data, linear static pressure distribution Eq. (8)
wall-wake representation of mean data, linear static pressure distribution, Eq. (8)
mean data, $\partial P/\partial y = 0$, Eq. (8)
wall-wake representation of mean data, $\partial P/\partial y = 0$, Eq. (8)
mean data, locally similar, linear static pressure distribution
wall-wake representation, locally similar, linear static pressure distribution
τ_w computed from wall-wake profile
y, cm
2.5
2.0
1.0
0.5
0.0
0.5
1.0
1
1
$[(\tau - \mu\partial u/\partial y)/\rho_e u_e^2] \times 10^3$

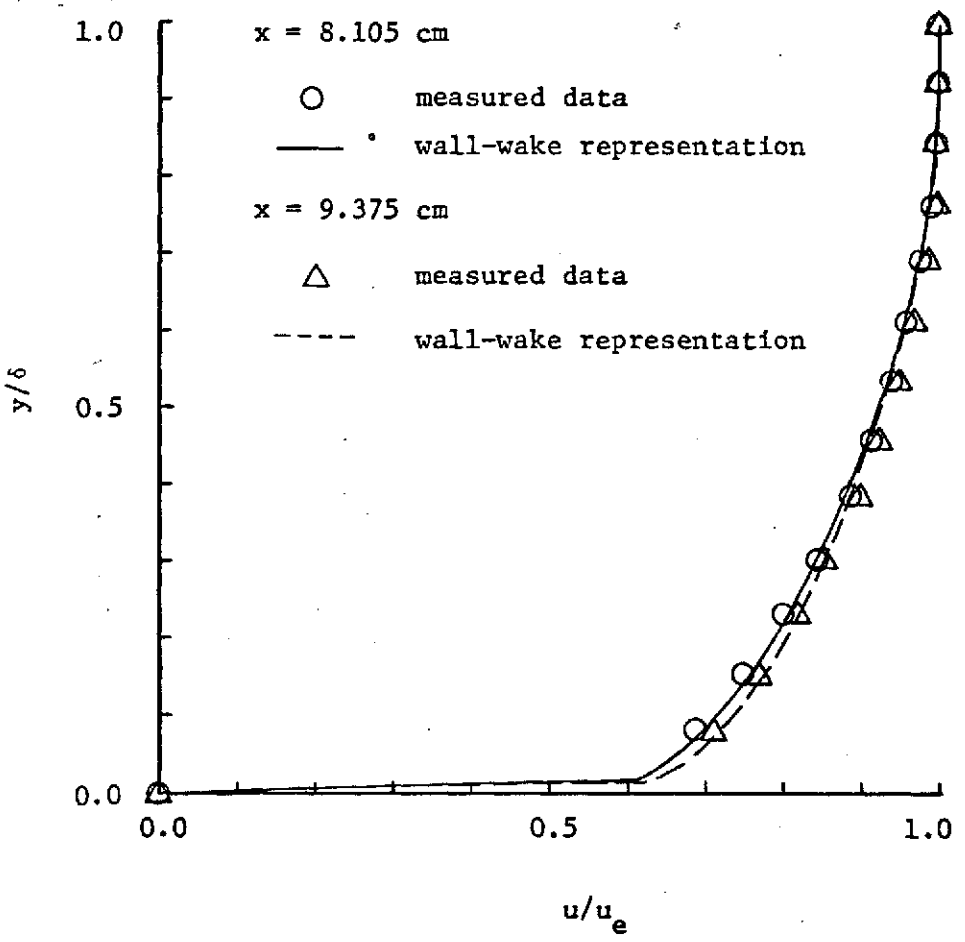
x = 8.105 cm
measured data
wall-wake representation
x = 9.375 cm
measured data
wall-wake representation
1.0
0.5
0.0
y/δ
0.0
0.5
1.0
u/u_e

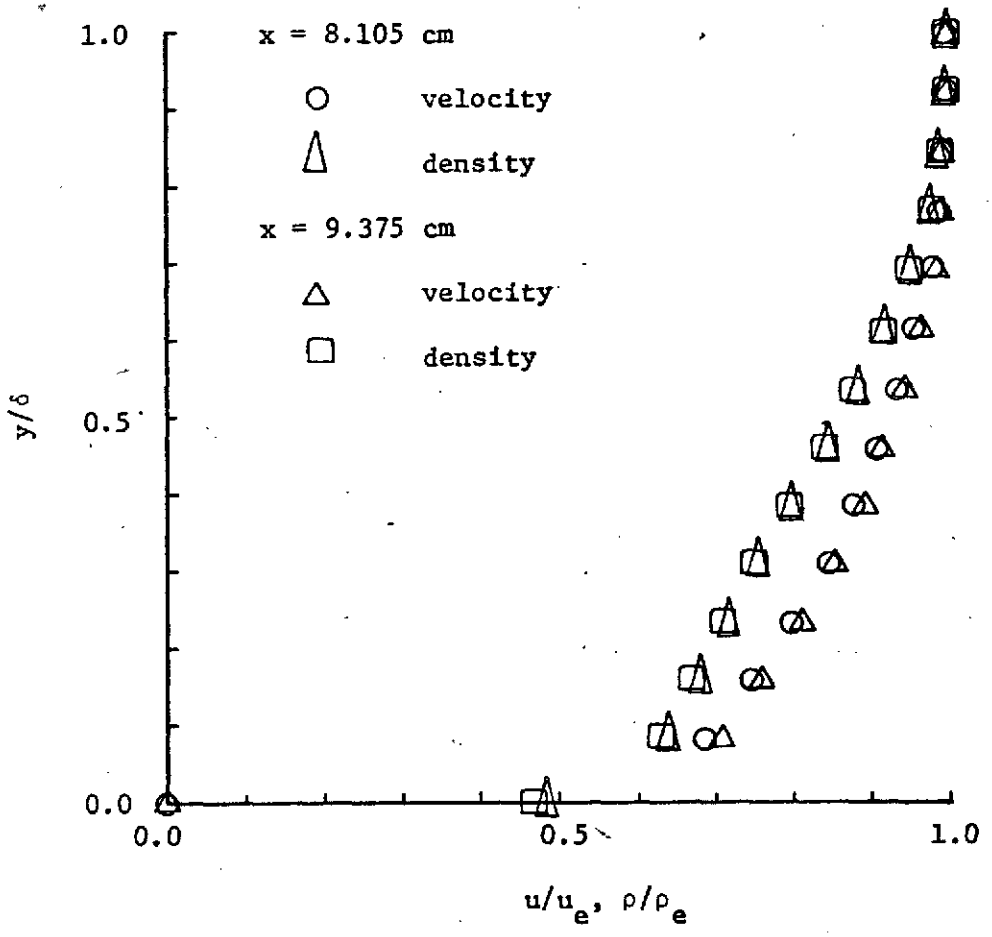
x = 8.105 cm
velocity
density
x = 9.375 cm
velocity
density
1.0
0.5
0.0
y/δ
0.0
0.5
1.0
u/u_e, ρ/ρ_e

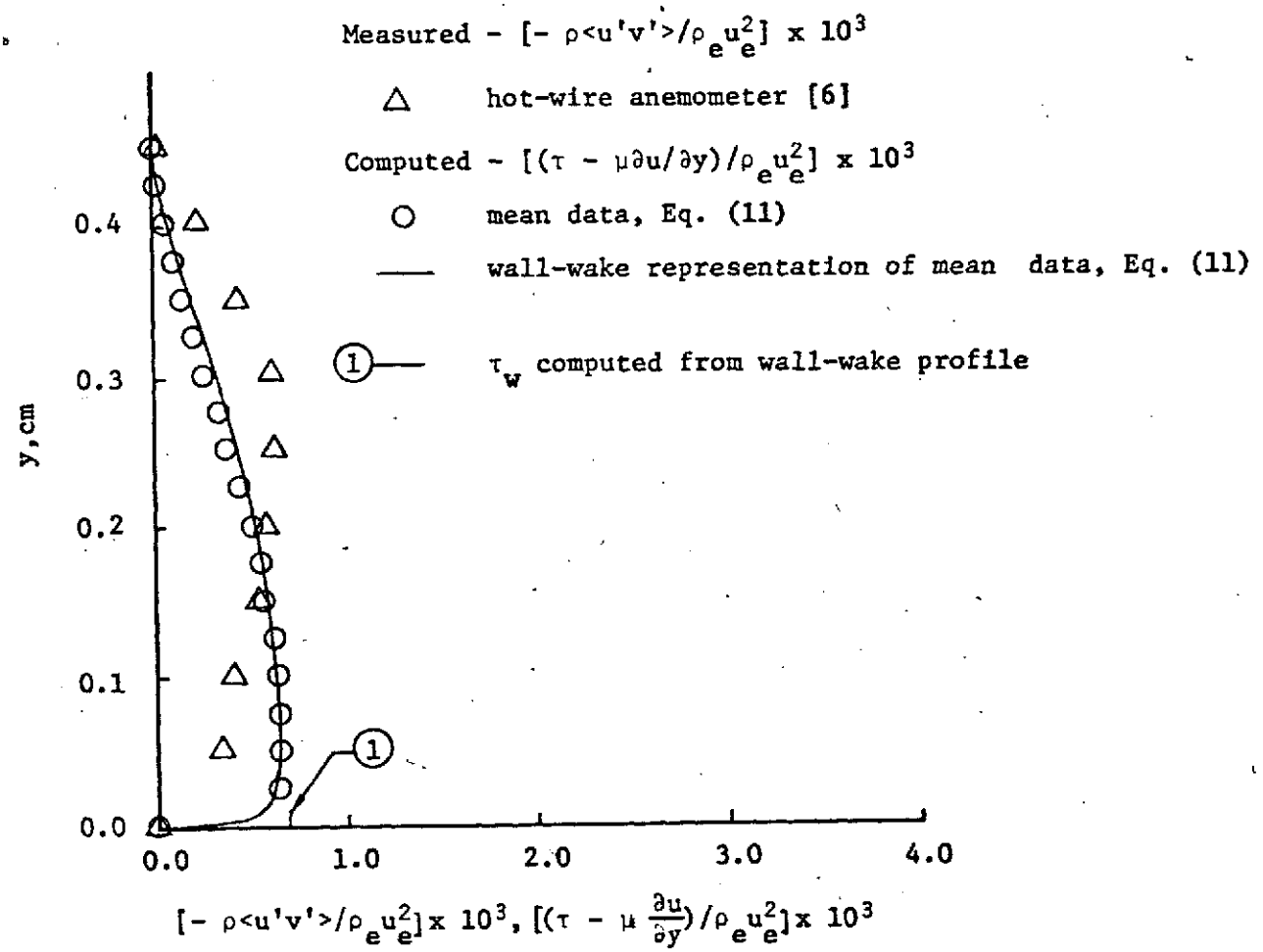
Measured - $[-\rho\langle u'v'\rangle/\rho_e u_e^2] \times 10^3$
hot-wire anemometer [6]
Computed - $[(\tau - \mu\partial u/\partial y)/\rho_e u_e^2] \times 10^3$
mean data, Eq. (11)
wall-wake representation of mean data, Eq. (11)
1
τ_w computed from wall-wake profile
y, cm
0.0
0.1
0.2
0.3
0.4
0.0
1.0
2.0
3.0
4.0
$[-\rho\langle u'v'\rangle/\rho_e u_e^2] \times 10^3$, $[(\tau - \mu \frac{\partial u}{\partial y})/\rho_e u_e^2] \times 10^3$

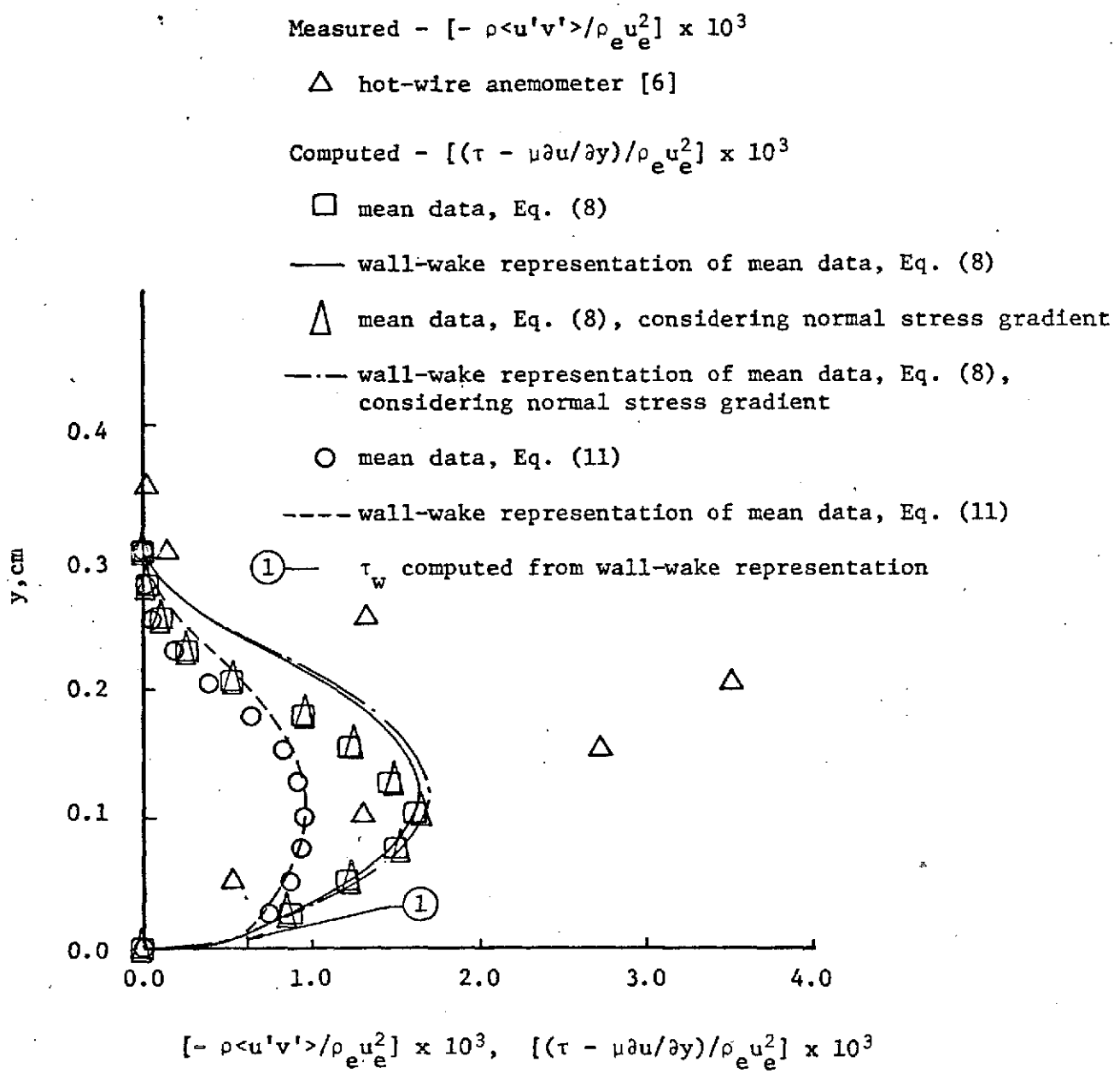
Measured - $[-\rho\langle u'v'\rangle/\rho_e u_e^2] \times 10^3$
hot-wire anemometer [6]
Computed - $[(\tau - \mu\partial u/\partial y)/\rho_e u_e^2] \times 10^3$
mean data, Eq. (8)
wall-wake representation of mean data, Eq. (8)
mean data, Eq. (8), considering normal stress gradient
wall-wake representation of mean data, Eq. (8), considering normal stress gradient
mean data, Eq. (11)
wall-wake representation of mean data, Eq. (11)
1 τ_w computed from wall-wake representation
y, cm
0.0
0.1
0.2
0.3
0.4
0.0
1.0
2.0
3.0
4.0
$[-\rho\langle u'v'\rangle/\rho_e u_e^2] \times 10^3$, $[(\tau - \mu\partial u/\partial y)/\rho_e u_e^2] \times 10^3$

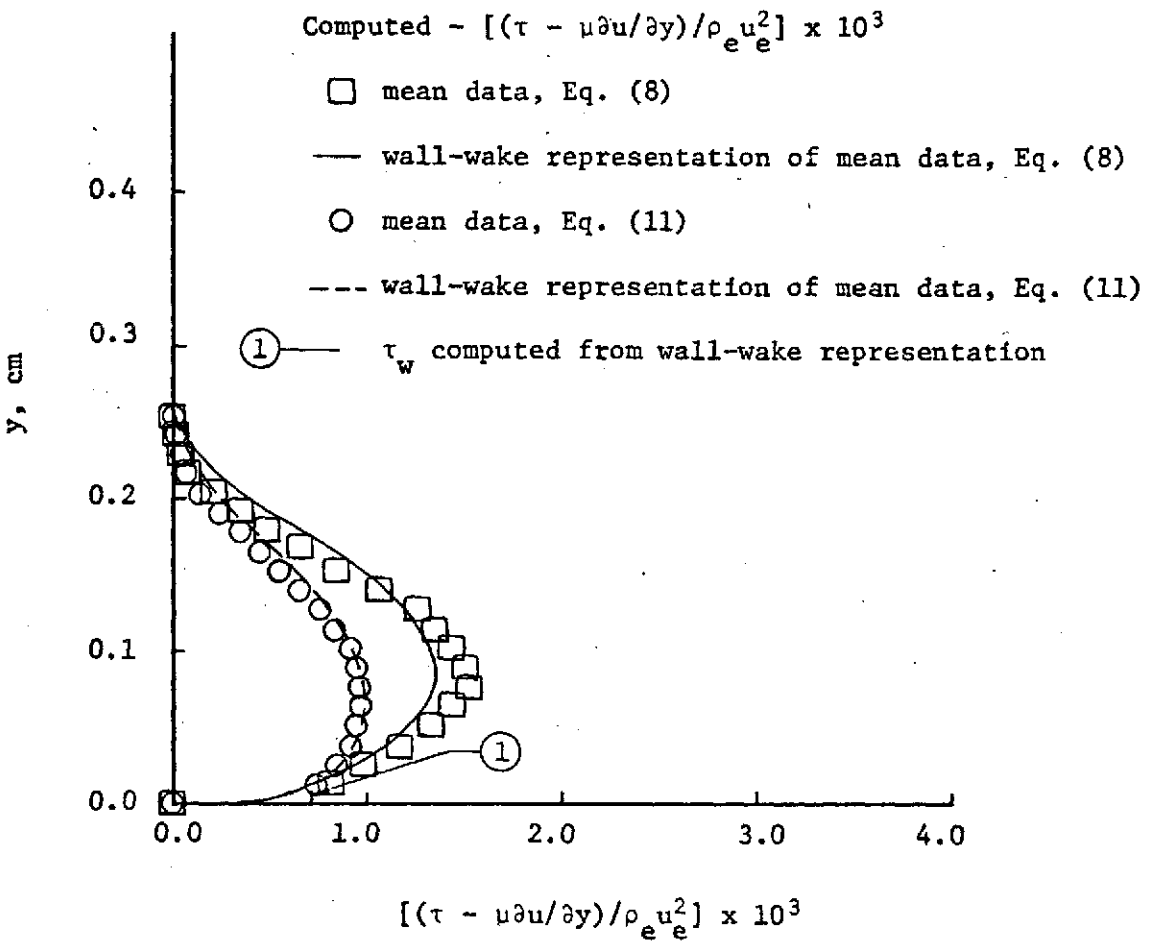
Computed - $[(\tau - \mu\partial u/\partial y)/\rho_e u_e^2] \times 10^3$
mean data, Eq. (8)
wall-wake representation of mean data, Eq. (8)
mean data, Eq. (11)
wall-wake representation of mean data, Eq. (11)
1 τ_w computed from wall-wake representation
y, cm
0.0
0.1
0.2
0.3
0.4
0.0
1.0
2.0
3.0
4.0
$[(\tau - \mu\partial u/\partial y)/\rho_e u_e^2] \times 10^3$

Eddy Viscosity based on measured shear stress

- ● x = 5.375 cm, laser velocimeter [4]
- ○ x = 9.375 cm, laser velocimeter [5]
- ▲ x = 5.375 cm, hot-wire anemometer
- △ x = 9.375 cm, hot-wire anemometer

Eddy Viscosity based on computed shear stress

- ■ x = 5.375 cm, computed from mean data, Eq. (8)
- □ x = 9.375 cm, computed from mean data, Eq. (8)
- —— x = 5.375 cm, computed from wall-wake representation of mean data, Eq. (8)
- ---- x = 9.375 cm, computed from wall-wake representation of mean data, Eq. (8)

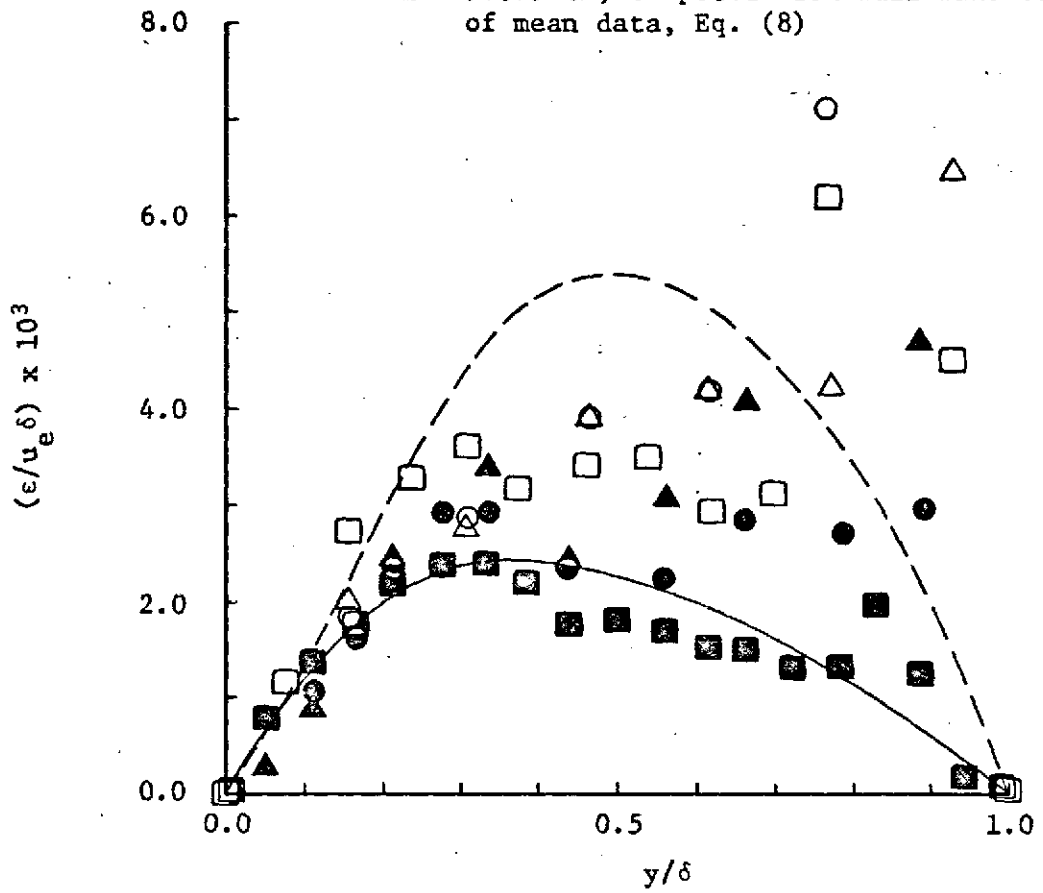

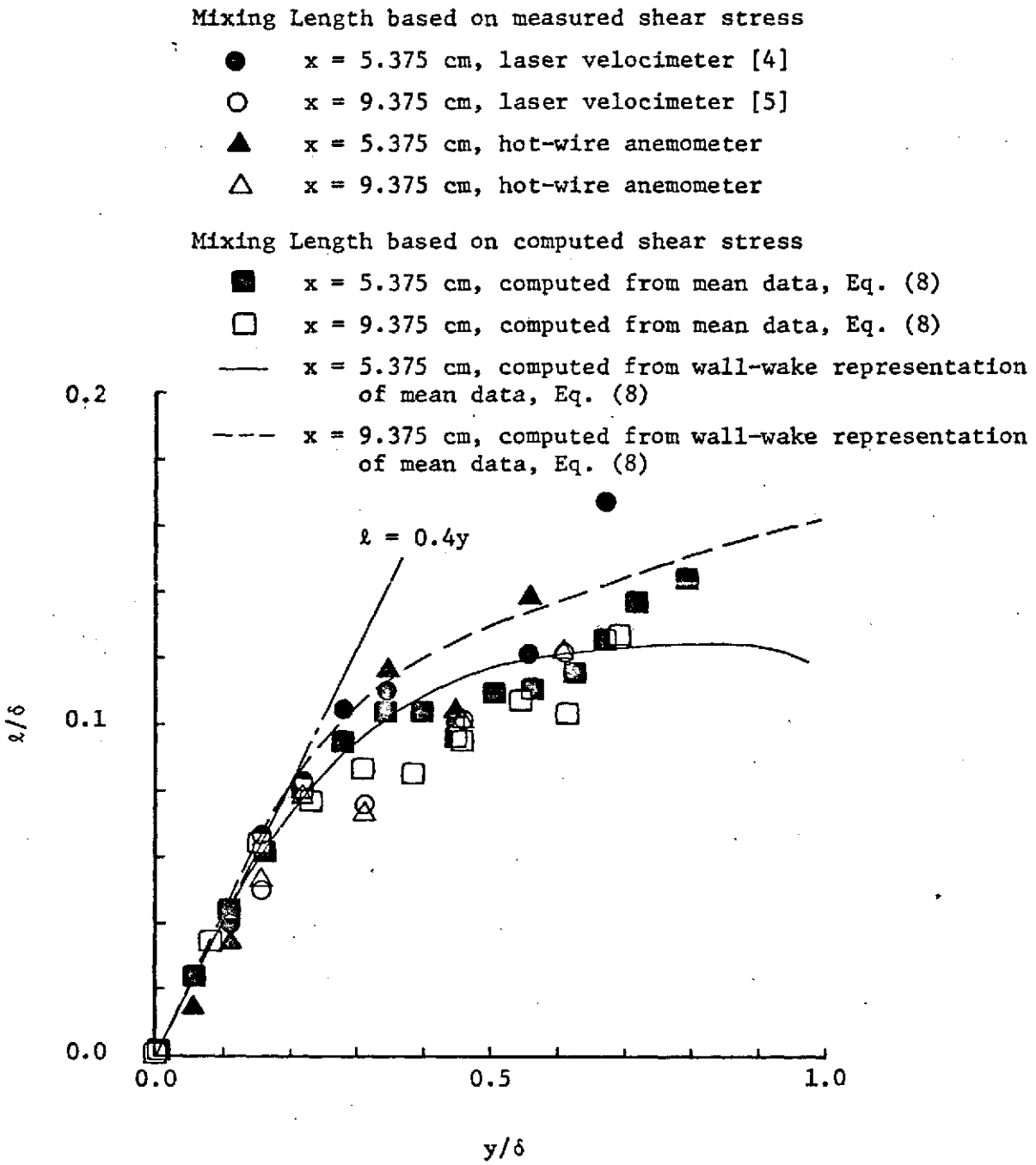
Mixing Length based on measured shear stress
x = 5.375 cm, laser velocimeter [4]
x = 9.375 cm, laser velocimeter [5]
x = 5.375 cm, hot-wire anemometer
x = 9.375 cm, hot-wire anemometer
Mixing Length based on computed shear stress
x = 5.375 cm, computed from mean data, Eq. (8)
x = 9.375 cm, computed from mean data, Eq. (8)
x = 5.375 cm, computed from wall-wake representation of mean data, Eq. (8)
x = 9.375 cm, computed from wall-wake representation of mean data, Eq. (8)
ℓ = 0.4y
0.2
0.1
0.0
ℓ/δ
0.0
0.5
1.0
y/δ

Eddy Viscosity based on measured shear stress

▲ x = 6.60 cm, hot-wire anemometer [6]

△ x = 10.16 cm, hot-wire anemometer [6]

Eddy Viscosity based on computed shear stress

● x = 6.60 cm, computed from mean data [6]

—— x = 6.60 cm, computed from wall-wake representation of mean data

○ x = 10.16 cm, computed from mean data [6]

– – – x = 10.16 cm, computed from wall-wake representation of mean data [6]

□ x = 9.62 cm, computed from mean data [9]

—·—· x = 9.62 cm, computed from wall-wake representation of mean data [9]

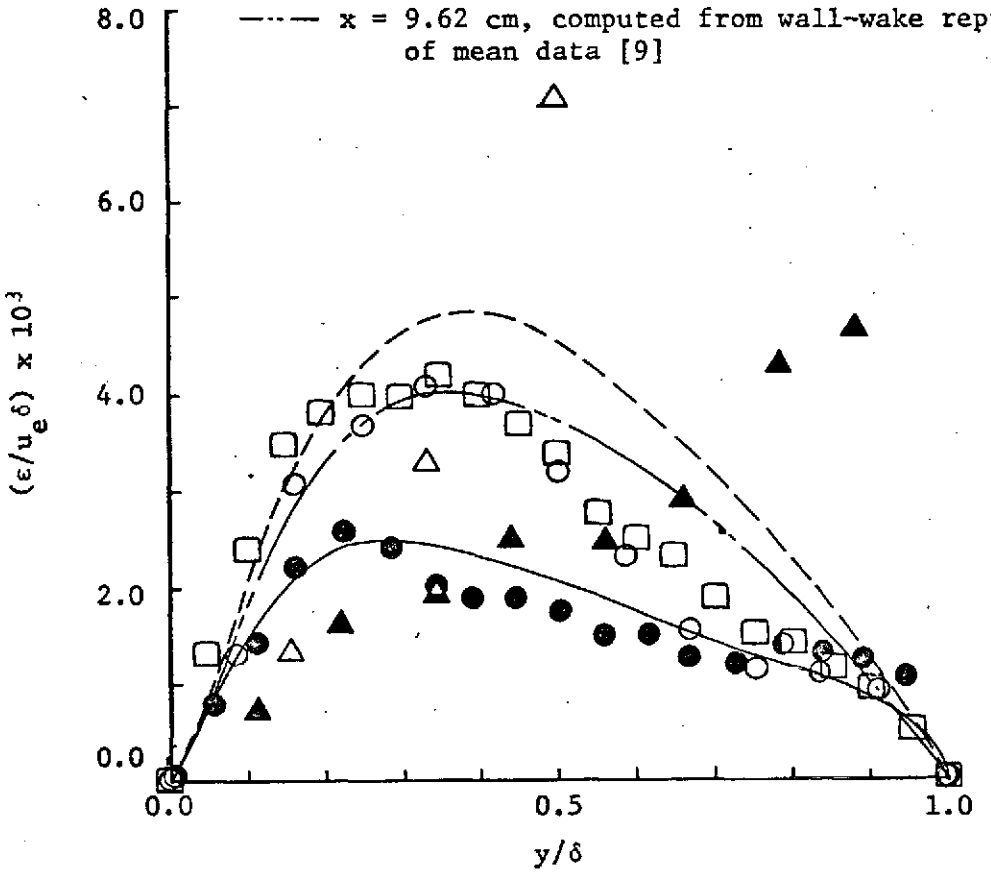

Mixing Length based on measured shear stress

▲ x = 6.60 cm, hot-wire anemometer [6]

△ x = 10.60 cm, hot-wire anemometer [6]

Mixing Length based on computed shear stress

● x = 6.60 cm, computed from mean data [6]

—— x = 6.60 cm, computed from wall-wake representation of mean data [6]

○ x = 10.16 cm, computed from mean data [6]

--- x = 10.16 cm, computed from wall-wake representation of mean data [6]

□ x = 9.62 cm, computed from mean data [9]

—·— x = 9.62 cm, computed from wall-wake representation of mean data [9]